PHYSICAL REVIEW B **80**, 165404 (2009)

Imaging the atomic orbitals of carbon atomic chains with field-emission electron microscopy

I. M. Mikhailovskij,* E. V. Sadanov, T. I. Mazilova, V. A. Ksenofontov, and O. A. Velicodnaja
Department of Low Temperatures and Condensed State, National Scientific Center, Kharkov Institute for Physics and Technology, Academicheskaja, 1, Kharkov 61108, Ukraine

(Received 17 July 2009; revised manuscript received 2 September 2009; published 7 October 2009)

A recently developed high-field technique of atomic chains preparation has made it possible to attain the ultrahigh resolution of field-emission electron microscopy (FEEM), which can be used to direct imaging the intra-atomic electronic structure. By applying cryogenic FEEM, we are able to resolve the spatial configuration of atomic orbitals, which correspond to quantized states of the end atom in free-standing carbon atomic chains. Knowledge of the intra-atomic structure will make it possible to visualize generic aspects of quantum mechanics and also lead to approaches for a wide range of nanotechnological applications.

DOI: 10.1103/PhysRevB.80.165404 PACS number(s): 61.05.−a, 68.37.Vj, 81.07.Vb

I. INTRODUCTION

Carbon atomic chains have remarkably high stability and failure-current density, and are therefore especially promising in all-carbon molecular electronics. In all reported approaches to realize free-standing carbon atomic chains, high-resolution microscopy has been exploited in process controls and structural analysis.[1–4] Field-emission electron microscopy[5] and scanning tunneling microscopy (STM),[6,7] in particular, have been used to direct probe the local density of states (LDOS) of single atoms, but the symmetry of the electronic states could be inferred only indirectly and the intra-atomic electronic structure or the shapes of atomic orbitals are only known from theoretical investigations. At present, there are several kinds of microscopes that are characterized by atomic resolution in routine operating regimes. They are the field-ion microscope (FIM), the scanning tunneling microscope in its various instrumental forms, and the high-resolution electron microscopy. Scanning tunneling spectroscopy and field-emission electron microscopy provides a direct method to probe the discrete electronic structure of nanoobjects.[7–10] Low-temperature ultrahigh-vacuum STM (Ref. 6) and FEEM (Ref. 5) can be used to perform atomically localized spectroscopic measurements of a single atom. FEEM enables the observation single quantum dots (molecules and atomic clusters). The organic molecules are represented on the phosphor screen by bright multiplets or some irregularly shaped FEEM images, known as molecular patterns.[11–13] The visibility of atoms in the FEEM was strongly evidenced in the few special cases.[5,14] However, FIM, STM, and FEEM images of the single atoms look like relatively wide structureless spots. These images of single atoms can be approximated by a simple Gaussian distribution, and hence it is more argued to consider such a situation in recent atomic-resolution microscopy as detecting a single atom rather than obtaining its real image. To date, there have been no reported experimental observations of the spatial form of the atomic orbitals.

Each of these atomic-resolution microscopes requires specimens with different configurations. The resolution of an FEEM decisively depends on the geometry of sample, which determines the field-enhancement factor above its tip. There is general trend toward enhancement of the FEEM resolution with the miniaturization of pointed specimens.[14,15] The recent progress in the carbon atomic chain preparation,[2] has made it possible to attain the extremely large field-enhancement factors corresponding to subangstrom resolution of a field-ion microscope.[16,17] The finite one-dimensional atomic chains, nanotubes, and graphene nanoribbons exhibit peculiar electronic end states localized at their termini,[10,18] which hold significant promise for future nanoelectronic device applications. Scanning tunneling spectroscopy measurements revealed the formation of quantized electronic end states, which transform the energy levels and the LDOS within the surface-supported finite atomic chains.[10] However the space configuration of wave functions of end states has not been characterized experimentally.

II. METHODS

Experiments were performed with the FEEM operating at 4.2 K in ultrahigh vacuum. An individual image spot on the microscope screen is formed by beam of electrons originating at the end atom of the chain [Fig. 1(a)]. Experimental procedures included *in situ* fabrication of atomic chains supported by the parabolic carbon tip of less than 1 μm radius are described before in details.[16,17] The controlled formation of carbon atomic chains on the apex of mesoscopic tips has been obtained by the high-field unraveling mechanism.[19] The atomic chains were fabricated at low temperatures under high-vacuum conditions by the application of positive electric field in a voltage range 1–15 kV. During this treatment the electric field was maintained constant at a level of 10^{11} V/m. All FEM experiments were performed in ultrahigh-vacuum chamber with a 1×10^{-7} Pa base pressure. The ultrahigh-vacuum conditions prevented the residual gas atoms from striking the surface under study. The migration of residual gases adsorbed on the surface of the chain and supporting carbon tip was strongly suppressed by deep freezing. A microchannel plate with a phosphor screen was used as an anode. The effective diameter of the screen was 60 mm. Local current characteristics of the field-electron emission were determined through digital microphotometry in order to avoid the uncertainties connected with secondary emission at high voltages in the complex conditions of a

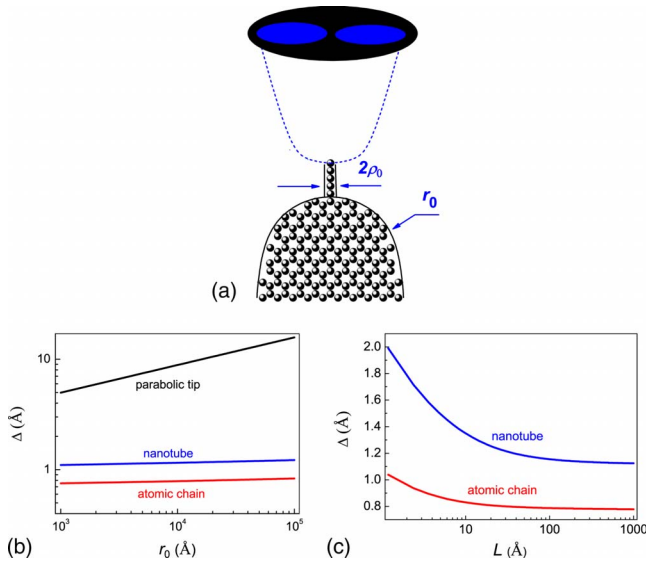

FIG. 1. (Color online) Characterization of high-resolution field-emission electron microscopy. (a) A schematic drawing of electron emission from a self-standing atomic chain anchored at the graphite parabolic tip, mounted opposite a luminescent screen. (b) The dependence of theoretical resolution of FEEM on the radius of the supporting parabolic electrode for carbon atomic chains, closed carbon nanotubes with fullerene end caps and conventional parabolic emitters. (c) The calculated resolution of FEEM as a function of the length of carbon atomic chains and nanotubes.

field-emission microscope. Image-intensity variations on the screen reflect the transverse field-emission density variations at the chain terminus. To get statistically relevant information on peculiarities of FEEM images of the atoms of atomic chains and to prove reliability of the method, we investigated 41 different carbon atomic chains produced during high-field treatment. The distribution of the atomic chain length directly calculated from the compression factor has a mean value of 5.9 nm, with a variance of 2.5 nm.

To examine the atomic chain formation in high electric fields, we carried out calculations of the graphene unraveling. The numerical simulations were carried out using the classical molecular-dynamics (MD) method, employing the short-range Tersoff-Brenner bond order potential.[20] The electric force producing an axial tension is localized at the top of the chain. In our molecular dynamics modeling the electric force was 0.2–6.0 nN. The time unit is 3.526×10^{-14} s and the time step is 7.052×10^{-16} s. The nonbonded interactions between the graphite monolayers (graphenes) determined by weak van der Waals forces were neglected in our simulation. The graphene sheet model used in the computations contains 33 interacting and 30 boundary atoms arranged in the same manner as in the "zigzag" nanotube. Computer modeling employed rigid boundary conditions on the lateral graphene edges. Boundary atoms were kept on lattice sites. The model is stable with respect to both homogeneous strain and phase transformation.

III. RESULTS AND DISCUSSIONS

Free-standing carbon atomic chains attached to the sharpened carbon fibers are characterized by a high mechanical strength and may provide the ultimately dense atomic-scale field-electron emission. The subangstrom FIM image resolution of anchored carbon atomic chains made it possible to demonstrate the feasibility of quantum motion imaging of atomic chains and to visualize in real space their atomic wave functions near the ground quantum states.[17] The field-emission current can be calculated by multiplying the impingement rate of free electrons at the surface by appropriate penetration coefficient. As only the states lying near the Fermi level of chains contribute to the field-emission process, the supply of tunneling electrons in a FEEM is to a good approximation proportional to the density of electronic states,[15,21] and a two-dimensional imaging of the LDOS corresponds to a spatial mapping of wave function probability densities $|\psi|^2$

The FEEM pattern on the screen is not exactly sharp, because electrons emitted from any point at the specimen have a transverse velocity, which results in a scattering disk on the phosphor screen. The resolution of the FEEM can be expressed in terms of a parameter δ, which is defined as the minimal diameter of the image disk, divided by the magnification of the image M. There are at least three factors, which limit the resolution of the FEEM, namely, the velocity of an electron near the Fermi level, the momentum uncertainty, and the geometric magnification factor depending on the specimen end form. The resolution of FEEM images of nanoobjects characterized by $M > 10^6$ is dominated by the momentum uncertainty term.[14] In this approximation, the resolution is given by $\delta = (2\hbar\tau/m_e M)^{1/2}$, where m_e is the mass of the electron and τ is the time of flight from tip to screen. The time τ is almost exactly equal to the flight time of electrons at full energy eV, were e is the charge of the electron and V is the applied potential. A carbon atomic chain can perfectly screen the applied electric field, resulting in sharp enhancement of the electric field at the end atom. To calculate the resolution of FEEM images of the carbon atomic chain on the needle-shaped electrode we used the "post on a paraboloid" model[17] [Fig. 1(a)], in which the chain stands normally on the parabolic electrode with the radius of curvature r_0, having a cylindrical shape of height l and closed with a hemispherical cap with radius $\rho_0 = 0.12$ nm.[21] Since the carbon atomic chain is conducting and hence an equipotential surface, line of force, and an initial part of trajectory are orthogonal to the effective electronic surface [Fig. 1(a)]. The lines of the force emerging from a chain are compressed after traveling normal to its surface for a short distance. The parabolic compression of the force line reduces the actual magnification. The image magnification of FEEM is proportional to the ratio of the specimen-to-screen distance R to the apex radius of the specimen ρ_0, that is: $M = R/\beta\rho_0$, where β is the image compression factor. In conventional FEEM of specimens described by a paraboloid, β is about 1.5, however, for one-dimensional chains on the tips this value is considerably understated.

Within the framework of this approximation, the compression factor is given by

$$\beta = \xi(r_0/L)^{1/2}, \tag{1}$$

where L is the total distance of the apex of the hemisphere from the paraboloid surface ($L = l + \rho_0$) and ξ is a numerical

constant which is almost independent of configurations of chains and supporting tips and has an approximate value of 1.145.[17] The apex field-enhancement factor for the chain on a paraboloid model is given by $\gamma=1.05(2+L/\rho_0)^{0.99}$. The field F at the end of the chain anchored at the apex of a paraboloidal tip can be shown to be $F=2\gamma V/r_0 \ln(2R/r_0)$. Using these expressions, the calculation yielded the following expression for the minimal diameter of resolved emission spots in FEEM images of free-standing linear nanoobjects:

$$\delta=(2\hbar\xi\rho_0)^{1/2}\left[\frac{em_e}{\gamma}LF\ln(2R/r_0)\right]^{-1/4}. \quad (2)$$

The field strength F in FEEM examinations of carbon atomic chains is usually varied in a narrow range about 10^9 V/m.[2] The resolution is determined by the uncertainty principle and the image magnification factor mostly depending on the radius ρ_0 and length L of the chain (nanotube). In spite of a partial image overlap, the two emission spots of diameter δ will just be resolved at positive values of the resolution ratio $\mu=(j_0-j_m)/j_0$, where j_0 and j_m are the electron current densities at the emission centers and the middle point between the two spots, correspondingly.[22] Field-emission single atom tips can be modeled by a cylindrical tube of radius $\delta/2$ with impenetrable walls,[23] and the emission probability density can be presented by the Bessel function of zero order. Within this approximation, the lateral resolution Δ is determined by the minimal distance between two emission spots corresponding to positive values of μ. For such a probability density Δ is equal to 0.46δ.

Figure 1(b) shows the change in the resolution given as a function of the radius of the supporting electrode for atomic chains, nanotubes, and parabolic specimens. The resolution of FEEM is determined largely by the radius of the tip ρ_0 and is affected only to a second order by the radius of the supporting electrode r_0. The dependence of resolution on the length [Fig. 1(c)] of a carbon atomic chain ($\rho_0=1.2$ Å) and a closed carbon nanotube with a fullerene end cap ($\rho_0=5.1$ Å) was calculated for typical conditions: $r_0=1\times10^{-6}$ m, $R=5\times10^{-2}$ m, and $F=5\times10^9$ V/m. At these conditions, the resolution for atomic chains and carbon nanotubes exceed those of conventional field-emission electron microscopy by an order of magnitude. The field strength, magnification, and resolution should all increase as the radius of the protrusion decreases. The application of columnar nanospecimens in FEEM drastically improved the resolution of the image to the subangstrom level, thus not only detecting a single atom would be expected, but also obtaining its spatial image or intra-atomic structure.

We use low-temperature FEEM to perform a systematic investigation of the shape of the wave function $|\psi(\rho,z,\varphi)|^2$. The overwhelming majority of FEEM images of the end atoms of carbon chains has symmetries presented in Fig. 2, which correspond to singlets and doublets of bright spots or occasionally to some odd-shaped patterns. The photographs in Figs. 2(a) and 2(b) were taken with an applied voltage 425 V and currents of 550 and 150 pA, respectively. The first field-emission electron image of the end atom has circular symmetric intensity distribution with maximum intensity at the center as expected for s-like states, while the second one

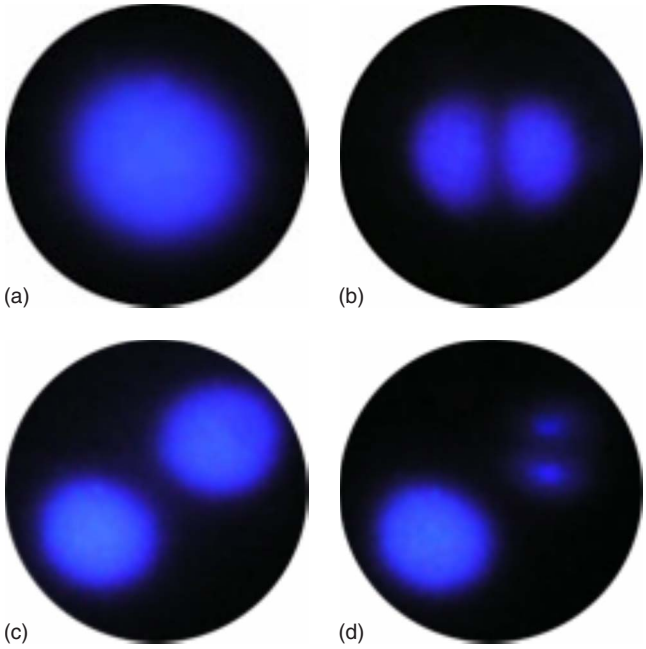

FIG. 2. (Color online) FEEM images of the end atoms of carbon chains. (a) Singlet and (b), doublet of bright spots were acquired with a voltage 425 V. The singlet patterns represent the most stable configuration. (c) s-like images of two atoms at the end of chains. (d) Spontaneous $s\rightarrow p$ transformation of the FEEM pattern at constant voltage of one of atoms shown in c.

has a pronounced node in the center as expected for p-like states. The extension angle of the FEEM image of the s-like patterns is equal to 0.12 ± 0.02 rad. This value is correspondent to the compression factor $\beta=17.4$ and the atomic chain length calculated from the Eq. (1) is equal to 4.33 nm.

Deletion or movement of only a portion of a FEEM pattern was never registered: singlet and doublet patterns always behaved as single units. Some of the singlet and doublet patterns disappeared within about ten second after they appeared. The rest of the localized FEEM patterns remained stable. At the electron current greater then 100 pA singlets occasionally change to doublets and vice versa. Figures 2(c) and 2(d) show representative patterns of two atoms, one of which spontaneously changes the FEEM image at constant voltage (440 V). This change corresponds to $s\rightarrow p$ transformation of the electronic orbital of the end atom. The configuration of the FEEM pattern of the second atom is invariable. The state without any node gives the largest current, i.e., the s-like state, gives a far larger current than p-like state with a node under the same voltage. Similarly, the pronounced field-emission current for the s-like states was recently obtained for an ultrathin metal nanowire.[24]

Another example of the mutual transformation of atomic FEEM images is shown in Fig. 3. The FEEM image in Fig. 3(a) has a truncated top with a small dent in its central region. Such a mixed FEEM pattern transforms successively to p-like and s-like states [(b) and (c) images]. The field-emission current from the end atom increases by two orders of magnitude at the $p\rightarrow s$ transformation. The two-dimensional spatial map of lines of equal brightness corresponding to the mixed FEEM pattern [Fig. 3(a)] is acquired

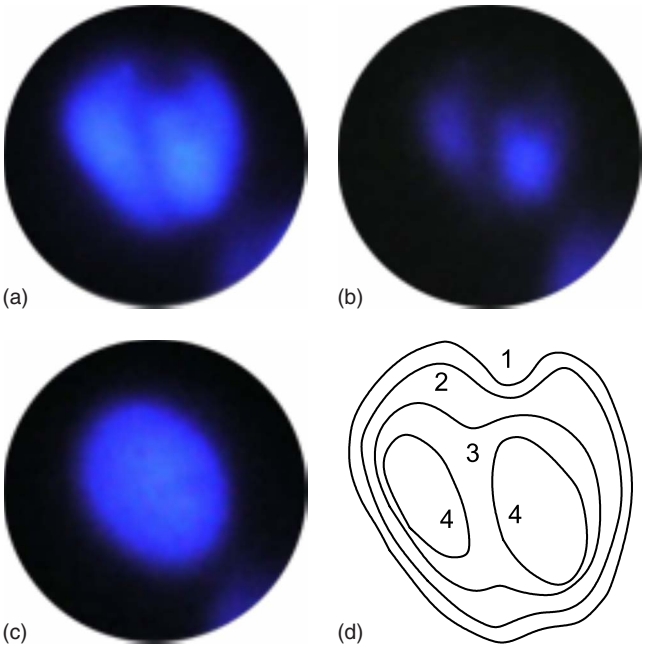

FIG. 3. (Color online) Transformation of atomic FEEM patterns. (a) A mixed FEEM state transforms successively to (b) *p*-like and (c) *s*-like states. The field-emission current from the end atom increases was increased by about 85 times at the $p \rightarrow s$ transformation. A considerable elliptical distortion of the FEEM patterns could be connected with the asymmetry of the supporting graphite tip. (d) A spatial map of lines of equal brightness corresponding to the mixed FEEM pattern (a).

using a high-resolution digital camera and digital frame grabbers with further computer processing. The brightness is proportional to electron current density j and normalized to their maximum value j_{m}. Lines 1–4 correspond to j/j_{m} equal to 0.20, 0.30, 0.45, and 0.50, respectively.

Bright singlet, doublet, and odd-shaped images of organic molecules were revealed before by the field-emission microscope.[11–13] So far, most of image mechanisms proposed to explain the molecular patterns fall into at least one of two categories, monomolecular,[11] and waveguide[13,25] models. In the waveguide models, which appear to explain most of the experimental results, the nature of molecular images is elucidated taking into account propagation of electronic waves along a cylindrical waveguide formed by the molecular complex. These models appear to explain some experimental results, but the mechanism of the spontaneous transformation of atomic FEEM patterns is unascertained. The observed in resent paper patterns are similar to field-emission images of single-walled carbon nanotubes[26] obtained in the investigation of emission states attributed to a chemisorbed molecule. However, the ultrahigh-vacuum conditions in our experiments, preliminarily cleaning the surface of the tips by field evaporation, and the suppression of the surface migration of impurities by cooling down to 4 K prevented the residual atoms from adsorption at the end of atomic chains.

To compare the observed squared wave functions to the ones that are obtained by calculations, we used the representation of the ground states of the linear carbon chains displaying axial symmetry by expanding the wave function ψ on a basis of a complete and orthogonal set of cylindrical wave functions[27] in the form

$$\psi_j(\mathbf{r}) = \sum_{G_\rho} \sum_{G_z} C_j(G_\rho, G_z) \Phi_{G_\rho G_z}(\mathbf{r}), \tag{3}$$

where G_ρ and G_z are wave vectors and the $\Phi_{G_\rho G_z}(\mathbf{r})$ are solutions of the Schrödinger equation

$$-\frac{\hbar^2}{2m}\nabla^2 \Phi_{G_\rho G_z}(\rho, z, \varphi) = \varepsilon_{G_\rho G_z} \Phi_{G_\rho G_z}(\rho, z, \varphi). \tag{4}$$

Here (ρ, z, φ) are cylindrical coordinates for free electrons confined inside a long cylindrical box of radius ρ_0 and $0 \leq \varphi \leq 2\pi$ and $0 \leq \rho \leq \rho_0$. The boundary conditions require that the total hence radial wave function vanish on the inner surface of the cylinder: $\Phi_{G_\rho G_z}(\rho_0, z, \varphi) = 0$. The motion of electrons along z direction is separable from the cross-sectional in-plane motion. The solution of the Schrödinger equation with these boundary conditions is given by the Bessel functions of the first kind of order n times a plane wave in z and an azimuthal phase factor:

$$\Phi_{G_r G_z}(\rho, z, \varphi) = e^{iG_z z} J_n\left(\rho \sqrt{\frac{2m_e E_\rho}{\hbar^2}}\right) e^{\pm in\varphi}, \tag{5}$$

where E_ρ is the radial component of kinetic energy of electron. The radial electron confinement leads to the quantization of the electron motion perpendicular to the chain with the radial quantization energies. The spectrum is determined by the discrete energies given by the eigenvalues $E_\rho^{n,i} = \hbar^2 X_{n,i}^2 / 2m_e \rho_0^2$, where $X_{n,i}$ denotes the i-th zero of Bessel function of order n.

Our results suggest that the field-emission electron patterns correspond to the shape of the squared wave functions of individual states with a circular intensity distribution as expected for an *s* state and with a pronounced node line in the center as expected for a *p* state. Calculations showed that $E_\rho^{0,1} < E_\rho^{1,1} \ll E_\rho^{0,2} < E_\rho^{1,2}$, and hence the higher angular momentum eigenstates can be ignored. Thus we can qualitatively explain the frequent occurrence of the FEEM patterns corresponding to *s* and *p* states. The distribution of local tunneling current above the nanoobjects generally represents the LDOS as plots of the probability density $|\Phi|^2$ in real space. It should be noted that in some special cases the local current depends on the spatial structure of the surface electronic tunneling barrier above molecules, which could be substantially anisotropic.[12] A comparison of experimental FEEM patterns (Figs. 2 and 3) with the theoretical calculations of the electron wave-function amplitude in carbon atomic chains (Fig. 4) shows a good agreement. We observe that the ground state and the first-excited state localized at the end atom have the expected *s*-like and *p*-like symmetries, respectively. Equations (3) and (5) successfully describe the wave function images we observe for *s*-like and *p*-like states [Figs. 4(a) and 4(b)]. The square of the *s* and *p* wave functions normalized to their maximum values. The predicted symmetry of the ground and first excited states corresponds to those observed by the low-temperature FEEM method. Similarly, an equal superposition of *s* and *p* eigenstates [Fig. 4(e)] appears consistent with the FEEM images of mixed

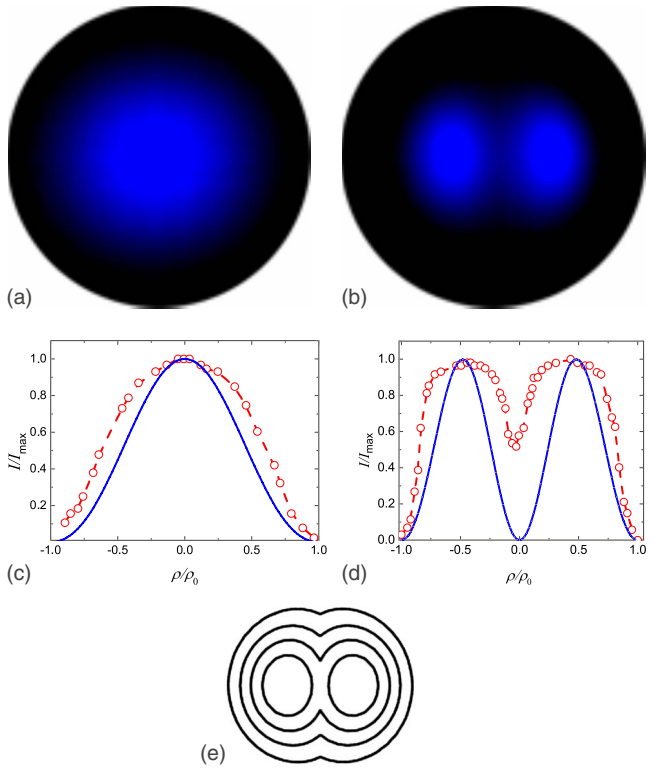

FIG. 4. (Color online) Spatial variations of squared wave functions of the end atom of the carbon chain. (a) and (b), FEEM image is formed by the calculated s and p orbitals, respectively. (c–e) Calculated maps of $|\Phi|^2$ based on Eqs. (3) and (5). The dashed and solid traces in (c), (d) indicate experimental data and calculation probability amplitudes of the eigenfunctions, respectively. The vertical axis is approximately proportional to the LDOS. (e) The calculated two-dimensional contour plot of the wave function density corresponding to an equal superposition of the s and p orbitals.

FEEM patterns [Figs. 3(a) and 3(d)]. The squared wave function $|\psi|^2$ in this state is thus a linear combination of the first two terms in the series Eq. (3).

An increase in field strength can cause a slight increase in the size and brightness of the doublets but a separation between any pairs of maximums is nearly constant and the ratio of this separation to the maximal diameter of the image spot equals to 2.11 ± 0.10. This ratio calculated from Eq. (5) is equal to 2.081 [Figs. 4(c) and 4(d)]. Coincidence of the experimental and calculated peaks and the close matching of a variety of calculated spatial patterns and FEEM images illustrate that some features of the orbitals of the end atom can be reproduced by Eq. (5). The increase in the spread of the intensity at the experimental peaks [Figs. 4(c) and 4(d)] can be attributed to a residual image smearing. The slight blurring of FEEM images can be due to the transverse momentum distribution of the field emitted electrons. It can be concluded that the FEEM patterns reflect the spatial distribution of the end electron states of a nanowire of an atomic-scale diameter. But the mechanism of the spontaneous $s \rightarrow p$ transformation at constant voltage remains unexplained.

To estimate a possible contribution of thermal vibrations to the blurring of FEEM images, the numerical simulations of mechanical oscillations of the carbon monoatomic chain

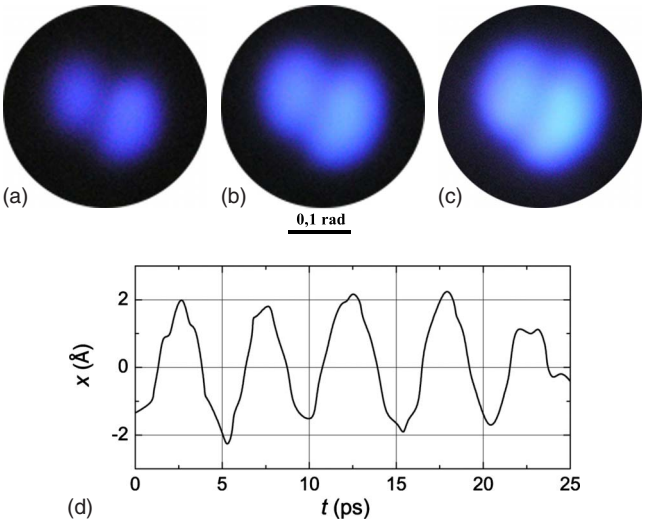

FIG. 5. (Color online) FEEM images of the end atoms of carbon chain at 300 K acquired with voltages (a) 330, (b) 340, and (c) 360 V. Thermal vibrations of the end atom of chain at this temperature shown in panel (d).

anchored to the graphene edge were performed using the molecular-dynamics method, employing the Tersoff-Brenner potential.[20] The chain was assumed to be in thermal contact with a macroobject at temperature T. The anchored atom of the chain every 8.85×10^{-15} s was reset to a new velocity adjusted to the Maxwell velocity distribution at T.[28] Typical thermal transverse oscillations of the carbon chain with $L = 1.12$ nm at 300 K are shown in Fig. 5. The main natural frequency for characteristic of the FEEM mode field strength of 5.0×10^9 V/m is 0.19 THz. The amplitudes of thermal vibrations of the free-standing carbon atomic chains are comparatively large (about 2 Å) and make a certain contribution (0.19 rad) to an enhancement of the electron emission angle at the tip. However, this value is substantially less then a typical field-emission angle $(2/3\pi)$ (Ref. 15) and exerts a small if any influence upon the blurring of FEEM images, even at a comparatively high temperature (300 K). Figures 5(a)–5(c) shows FEEM patterns of the end atoms of carbon chains at 300 K at field-electron currents (a) 7, (b) 20, and (c) 37 pA acquired with voltages 330, 340, and 360 V, respectively. A comparison of these images with those obtained at 4 K [Figs. 3(a) and 3(b)] shows the absence of substantial differences. At the same time the end atom of a chain is coupled

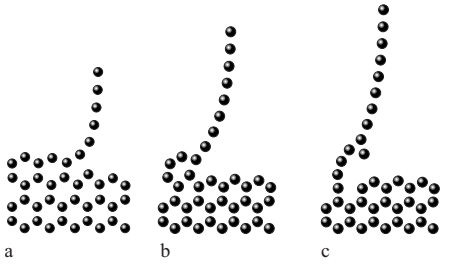

FIG. 6. Forming of the branched carbon nanowire during the unraveling of a graphene sheet. Labels (a)–(c) denote the various unraveling stages.

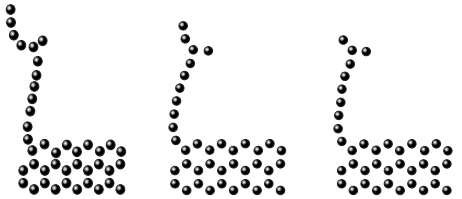

FIG. 7. Relaxed configuration of branched atomic chains with the numbers of carbon atoms equal to: 12 (a), 10 (b), and 9 (c).

with a graphene layer at low temperatures through quantized vibration of the supporting linear atomic chain,[17,29] and hence the detailed interpretation of the FEEM images requires careful theoretical consideration of the quantum linear support.

The angular symmetry of the *s* orbitals is transferred to the angular symmetry of the FEEM images [Figs. 2(a), 4(a), and 5(a)–5(c)]. A significant quasielliptical distortion of the FEEM images (Fig. 3) indicates that the violation of axial symmetry takes place. Taking into account that the radius of atomic chain ρ_0 is scores of orders of magnitude less than that of the supporting electrode r_0, a considerable elliptical distortion of the FEEM images could not be caused by the asymmetry of the supporting tip. We note that under the ultrahigh-field conditions the unraveling of graphene layers is quasiadiabatic and does not occur at constant temperature. The consequent contraction of the atomic bonds during unraveling causes an abrupt decrease of potential energy and atomic oscillations. The average amplitude of oscillations corresponds to temperature of about 10^4 K.[2,28]

Therefore, the unraveling proceeds in an ultrahigh-temperature surface region of carbon fibers. Due to explosive local overheating, atomic chains proved to be very nonequilibrium objects. In Fig. 6 snapshots of the unraveling dynamics of a single *C*-chain extending out from the graphene sheet: (a) at the beginning; (b) after 7.0×10^{-14} s, (c) after 1.41×10^{-13} s, and (d) 2.10×10^{-13} s are shown. The unraveling of graphene in high electric fields is accompanied by extraction of additional atoms—branching of atomic chains [Fig. 6(c)].

Figure 7 shows the branched atomic chains with the lengths of 9–12 atoms after relaxation after unraveling during 4.2×10^{-13} s. Relaxation of such nonlinear atomic chains led to significant violation of azimuthal symmetry of chain. This gives rise to the angular asymmetry in the FEEM images.

IV. CONCLUSIONS

Imaging the electron wave functions in reduced dimensions has allowed researchers to visualize generic aspects of quantum mechanics and has also led to new approaches for a wide range of nanotechnological applications. Field-emission electron microscopy and scanning tunneling microscopy have been used to direct probe the local density of states of single atoms, but the symmetry of the electronic states could be inferred only indirectly and the shapes of atomic orbitals are only known from theoretical investigations. Here we showed that a high-field technique of carbon atomic chains preparation has made it possible to attain the ultrahigh resolution of FEEM, which can be used to direct, real-space two-dimensional imaging the electronic orbitals of single atoms. We explore the opportunity for improving the spatial resolution of the FEEM images by miniaturization of pointed nanospecimens, approaching the atomic scale, and acquired the spatial distributions of emitted electrons from the end atoms of carbon chains. Atomic electronic states with *s* and *p* character are manifest in field-electron images as singlets and duplets patterns, which qualitatively agree with analytically calculated wave functions. By applying cryogenic FEEM, the spatial distribution of squared wave function of electrons, which corresponds to quantized states of the end atom in free-standing carbon atomic chains, was observed with subangstrom resolution.

Note added in proof. For reviews of ultrahigh resolution STM and AFM of atoms, see Ref. 30

We thank V. M. Azhazha, I. M. Neklyudov, V. I. Sokolenko, L. V. Tanatarov, and N. Wanderka for discussions and comments. This research was partially supported by the National Academy of Sciences of the Ukraine, Deutsche Forschungsgemeinschaft, and the NATO International Program.

*mikhailovskij@kipt.kharkov.ua

[1] T. D. Yuzvinsky, W. Mickelson, S. Aloni, G. E. Begtrap, A. Kis, and A. Zettl, Nano Lett. **6**, 2718 (2006).
[2] I. M. Mikhailovskij, N. Wanderka, V. A. Ksenofontov, T. I. Mazilova, E. V. Sadanov, and O. A. Velicodnaja, Nanotechnology **18**, 475705 (2007); in *Kharkov Nanotechnology Assembly-2007*, edited by I. M. Neklyudov, A. P. Shpak, and V. M. Shulaev (Kharkov Institute of Physics and Technology, Kharkov, 2007) Vol. 2, p.78.
[3] C. Jin, H. Lan, L. Peng, K. Suenaga, and S. Iijima, Phys. Rev. Lett. **102**, 205501 (2009).
[4] J. van Ruitenbeek, Physics **2**, 42 (2009).
[5] E. Rokuta, H.-S. Kuo, T. Itagaki, K. Nomura, T. Ishikawa, B.-L. Cho, I.-S. Hwang, T. T. Tsong, and C. Oshima, Surf. Sci. **602**, 2508 (2008).
[6] M. F. Crommie, C. P. Lutz, and D. M. Eigler, Phys. Rev. B **48**, 2851 (1993).
[7] E. E. Vdovin, A. Levin, A. Patanè, L. Eaves, P. C. Main, Yu. N. Khanin, Yu. V. Dubrovskii, M. Henini, and G. Hill, Science **290**, 122 (2000).
[8] S. G. Lemay, J. W. Janssen, M. van den Hout, M. Mooij, M. J. Bronikowski, P. A. Willis, R. E. Smalley, L. P. Kouwenhoven, and C. Dekker, Nature (London) **412**, 617 (2001).
[9] T. W. Odom, J.-L. Huang, P. Kim, and Ch. M. Lieber, Nature (London) **391**, 62 (1998).
[10] J. N. Crain and D. T. Pierce, Science **307**, 703 (2005).

[11] A. J. Melmed and E. W. Müller, J. Chem. Phys. **29**, 1037 (1958).
[12] G. R. Condon and J. A. Panitz, J. Vac. Sci. Technol. B **18**, 1216 (2000).
[13] T. A. Tumareva, G. G. Sominskiĭ, and A. S. Polyakov, Tech. Phys. **47**, 250 (2002).
[14] I. Brodie, Surf. Sci. **70**, 186 (1978).
[15] R. Gomer, *Field Emission and Field Ionization* (American Inst. of Physics, New York, 1993).
[16] I. M. Mikhailovskij, G. D. W. Smith, N. Wanderka, and T. I. Mazilova, Ultramicroscopy **95**, 157 (2003).
[17] T. I. Mazilova, I. M. Mikhailovskij, V. A. Ksenofontov, and E. V. Sadanov, Nano Lett. **9**, 774 (2009).
[18] A. K. Geim and K. S. Novoselov, Nature Mater. **6**, 183 (2007).
[19] A. G. Rinzler, J. H. Hafner, P. Nikolaev, L. Lou, S. G. Kim, D. Tomanek, P. Nordlander, D. T. Colbert, and R. E. Smalley, Science **269**, 1550 (1995).
[20] D. W. Brenner, Phys. Rev. B **42**, 9458 (1990).
[21] A. Lorenzoni, H. E. Roman, F. Alasia, and R. A. Broglia, Chem. Phys. Lett. **276**, 237 (1997).
[22] D. Sestovic and M. Sunjic, Phys. Rev. B **51**, 13760 (1995).
[23] J. Summhammer and J. Schmiedmayer, Phys. Scr. **42**, 124 (1990).
[24] Ch.-K. Lee, B. Lee, J. Ihm, and S. Han, Nanotechnology **18**, 475706 (2007).
[25] A. P. Komar and A. A. Komar, Sov. Phys. JETP **7**, 634 (1963).
[26] G. L. Martin and P. R. Schwoebel, Surf. Sci. **601**, 1521 (2007).
[27] M. Bianchetti, P. F. Bounsante, F. Ginnelli, H. E. Roman, R. A. Broglia, and F. Alasia, Phys. Rep. **357**, 459 (2002).
[28] Y. Wang, X.-J. Ning, Z. Z. Lin, P. Li, and J. Zhuang, Phys. Rev. B **76**, 165423 (2007).
[29] K. R. Brown, D. A. Lidar, and K. B. Whaley, Phys. Rev. A **65**, 012307 (2001).
[30] M. Herz, F. J. Giessibl, and J. Mannhart, Phys. Rev. B **68**, 045301 (2003); F. J. Giessibl and C. F. Quote, Phys. Today **59** (12), 44 (2006); http://blogs.nature.com/news/thegreatbeyond/2009/09/electron_clouds_seeing_is_beli.html